

Can Un-trained Neural Networks Compete with Trained Neural Networks at Image Reconstruction?

Mohammad Zalbagi Darestani* and Reinhard Heckel^{†,*}

*Dept. of Electrical and Computer Engineering, Rice University

[†]Dept. of Electrical and Computer Engineering, Technical University of Munich

July 7, 2020

Abstract

Convolutional Neural Networks (CNNs) are highly effective for image reconstruction problems. Typically, CNNs are trained on large amounts of training images. Recently, however, un-trained neural networks such as the Deep Image Prior and Deep Decoder have achieved excellent image reconstruction performance for standard image reconstruction problems such as image denoising and image inpainting, without using any training data. This success raises the question whether un-trained neural networks can compete with trained ones for practical imaging tasks. To address this question, we consider accelerated magnetic resonance imaging (MRI), an important medical imaging problem, which has received significant attention from the deep-learning community, and for which a dedicated training set exists. We study and optimize un-trained architectures, and as a result, propose a variation of the architectures of the deep image prior and deep decoder. We show that the resulting convolutional decoder outperforms other un-trained methods and—most importantly—achieves on-par performance with a standard trained baseline, the U-net, on the FastMRI dataset, a new dataset for benchmarking deep learning based reconstruction methods. Besides achieving on-par reconstruction performance relative to trained methods, we demonstrate that a key advantage over trained methods is robustness to out-of-distribution examples.

1 Introduction

CNNs are highly successful tools for image reconstruction tasks. In recent years, a large number of works have shown that they can outperform traditional image processing methods for tasks such as image denoising, compressive sensing, and image compression [Bor+17; The+17; Tod+15; Agu+17; Bur+12]. Almost exclusively, CNNs are trained on a large amount of images, and their success is typically attributed to their ability to learn from those training images.

However, starting with the Deep Image Prior (DIP) [Uly+18], a number of works have demonstrated that for a variety of inverse problems the architecture of a CNN acts as a sufficiently strong prior to enable image reconstruction, even without any training data. Un-trained networks perform well for denoising [Uly+18; HH19], compressive sensing [Vee+18], compressive sensing in magnetic resonance imaging [Aro+20], phase retrieval [JH19; Bos+20; Wan+20], and even for reconstructing videos [Jin+19; HA20]. Moreover, they provably succeed in denoising smooth signals and reconstructing smooth signals from few measurements [HS20a; HS20b].

This recent success raises the following question: *Can well-tuned un-trained neural networks compete with trained neural networks for important and practical image reconstruction problems?*

The goal of this paper is to address this question in the context of accelerated magnetic resonance imaging (MRI). MRI is an important medical imaging technique and is extremely popular because it is non-invasive. However, performing an MRI scan is relatively slow because of physical limitations of the scanning process. These limitations have led scientists to a line of research known as compressed sensing which focuses on accelerating MRI by reconstructing an image from a few measurements, which in turn results in a faster scan time.

Traditional Compressed Sensing (CS) methods are based on ℓ_1 -norm minimization and Total Variation (TV) norm minimization [Blo+07]. Those methods are implemented in modern MRI scanners, but are outperformed by an emerging class of deep-learning-based reconstruction techniques [Ye19]. Just last year,

a dedicated publicly available dataset for accelerated MRI has been introduced by Zbontar et al. [Zbo+18], named the FastMRI dataset, to enable MRI-specific training. Deep-learning methods for MRI typically require a significant amount of training time (days to weeks), yet at inference time, they are fast and yield excellent reconstruction quality.

Examples of deep-learning methods that perform well for accelerated MRI reconstruction include the U-net [Ron+15], Pyramid Convolutional Recurrent Neural Network (CRNN) [Wan+19], Cascade net [Sch+17], and invertible Recurrent Inference Machines (i-RIM) [PW19]. In this paper, we focus on the U-net as a baseline for trained methods, because of its popularity and ease of use. The U-net is also a baseline in the FastMRI challenge [Zbo+18]. We note, however, that the U-net is (slightly) outperformed by the aforementioned more tailored neural networks.

In this work we study popular un-trained neural network architectures for accelerated MRI reconstruction and propose a new one that yields on-par performance with the U-net. In more detail, our contributions are:

- We propose a variation of the deep image prior [Uly+18] and deep decoder [HH19] architectures, called ConvDecoder, and show that the ConvDecoder performs best for MRI imaging. The ConvDecoder is a simple convolutional generator comprised only of up-sampling, convolution, batch normalization, and ReLU blocks in each layer.
- We show that the ConvDecoder significantly outperforms traditional un-trained methods (i.e., TV-minimization) and, perhaps surprisingly, has on-par performance with the U-net trained on the FastMRI dataset. This suggests that there is less benefit in learning-based approaches for imaging, at least in the context of MRI, than currently thought.
- Finally, we demonstrate that a key advantage of un-trained methods over trained ones is robustness to out-of-distribution examples: At inference time, trained methods—unlike un-trained methods—are often not robust to a shift in the distribution, as demonstrated in Section 6.

2 Problem statement: Accelerated MRI

We start by formally stating the inverse problem on which we choose to evaluate un-trained methods, that is, accelerated multi-coil MRI reconstruction. Our goal is to recover an image $\mathbf{x} \in \mathbb{C}^N$ from a set of measurements. The measurements are obtained as

$$\mathbf{y}_i = \mathbf{MFS}_i\mathbf{x} + \text{noise}, \quad i = 1, \dots, n_c,$$

where \mathbf{S}_i is a complex-valued position-dependent sensitivity map, that is applied through entry-wise multiplication to the image \mathbf{x} , \mathbf{F} implements the 2D discrete Fourier transform, n_c is the number of magnetic coils, and \mathbf{M} is a mask that implements under-sampling. The measurements \mathbf{y}_i are called k -space measurements.

First, suppose that we are only given one measurement, this is called single-coil imaging. Also, suppose that the sensitivity map is equal to identity, and that the mask also corresponds to the identity, i.e., we are given a single measurement $\mathbf{y} = \mathbf{F}\mathbf{x} + \text{noise}$. In this case, we can estimate the image up to the uncertainty of the additive noise as $\hat{\mathbf{x}} = \mathbf{F}^{-1}\mathbf{y}$. In accelerated imaging, the k -space is under-sampled which is modeled through multiplication with the mask \mathbf{M} which simply sets some of the frequencies of the k -space measurement to zero. Under-sampling by a factor of K results in a scan speed-up by the same factor. Reconstruction from the under-sampled measurements amounts to estimating an image from few measurements which is known as compressed sensing.

The practically most relevant problem is multi-coil reconstruction. In multi-coil imaging, each of the sensitivity maps results in a different measurement. The sensitivity maps are often not given, but can be estimated from the measurements. In this paper we consider the problem of reconstructing an image from under-sampled multi-coil measurements.

We work with the recently released FastMRI dataset [Zbo+18]. The FastMRI dataset consists of a training and validation set each consisting of full k -space measurements of knees taken with $n_c = 15$ coils.

The dataset also contains “reference” images which are obtained by reconstructing an image from each coil measurement as $\hat{\mathbf{x}}_i = \mathbf{F}^{-1}\mathbf{y}_i$ and then combining those estimates via the root-sum-of-squares (RSS) algorithm to a final image:

$$\hat{\mathbf{x}} = \sqrt{\sum_{i=1}^{n_c} |\hat{\mathbf{x}}_i|^2}. \quad (1)$$

Here, $|\cdot|$ and $\sqrt{\cdot}$ denote element-wise absolute value and squared root operations. Because different coil sensitivities overlap only little, the RSS algorithm works well for combining the images.

We consider accelerated imaging by obtaining measurements with a mask. We utilize a standard 1D variable-density mask (i.e., random vertical lines across the k -space), because those masks are challenging but practically most relevant, and are the default in the FastMRI challenge. For evaluation, we compare to the “reference” images reconstructed from the full k -space.

3 Image recovery with un-trained neural networks

In this section, we discuss image recovery with un-trained neural networks. We view un-trained neural networks as convolutional image priors mapping a parameter space to image space, i.e., $G: \mathbb{R}^p \rightarrow \mathbb{R}^{c \times w \times h}$, where c is the number of channels of the output image (for example $c = 1$ for single grayscale image), and w and h are the width and height of the output image, respectively. Deep-learning-based image models are typically trained; specifically, they are parameterized functions mapping an input to an output, with trainable (weight) parameters. For such trained image priors, the input parameterizes the image, the output is an image, and the weights are the trainable parameters. In contrast, an un-trained neural network is an image model where the input to the network is relatively irrelevant and fixed, the weights are the parameters of the model, and the output of the model is again an image.

As mentioned before, un-trained neural networks have been proposed first for image restoration problems by Ulyanov et al. [Uly+18]. Ulyanov et al. [Uly+18] proposed to use a simple U-net architecture consisting of an encoder, decoder, and skip connections for image reconstruction by fitting this architecture to a measurement. It has relatively quickly been realized that the encoder and the skip connections are irrelevant for the performance of this methodology.

3.1 Single-coil reconstruction

Let $\mathbf{y} \in \mathbb{C}^M$ be the under-sampled k -space measurement and let \mathbf{MF} be the mask and Fourier transform defined in Section 2 that maps an image to a measurement. Given an un-trained neural network $G: \mathbb{R}^p \rightarrow \mathbb{R}^{c \times w \times h}$ with parameter vector $\mathbf{C} \in \mathbb{R}^p$, we estimate an image based on the measurements \mathbf{y} by first minimizing the mean-squared loss function

$$\mathcal{L}(\mathbf{C}) = \frac{1}{2} \|\mathbf{y} - \mathbf{MFG}(\mathbf{C})\|_2^2, \quad (2)$$

with gradient descent to obtain the estimate $\hat{\mathbf{C}}$, and second, estimating the image as $\hat{\mathbf{x}} = G(\hat{\mathbf{C}})$. The image consists of a real and imaginary part, each described by one channel, therefore $c = 2$. We elaborate on multi-coil reconstruction with an un-trained image model next.

3.2 Multi-coil accelerated MRI reconstruction

In multi-coil imaging, multiple magnetic coils take different k -space measurements of the same image. Therefore, there are a variety of approaches to use un-trained methods for image reconstruction. The most obvious one is to treat each measurement/coil independently, reconstruct as described in the single-coil reconstruction section above, and then combine the images using the RSS algorithm in equation (1).

A better approach is to impose the same prior to all images pertaining to the coils. This approach was first used by Arora et al. [Aro+20]. In this case, the first two output channels of the un-trained network generate the real and imaginary parts of the first image, the second two channel generate the the real and imaginary parts of the second image and so on. The final single image is then obtained again using the RSS algorithm in equation (1). In this case, the loss function in 2 changes to

$$\mathcal{L}(\mathbf{C}) = \frac{1}{2} \|\mathbf{Y} - \mathbf{MFG}(\mathbf{C})\|_F^2, \quad (3)$$

where \mathbf{Y} contains n_c (number of coils) under-sampled measurements rather than one. We found that using a single image prior for all images as explained above gives slightly better reconstruction quality and is significantly more efficient (approximately nine times faster), and hence we proceed with this second approach.

4 Network architectures

In this section we discuss the network architectures we consider in this paper. All architectures we considered for MRI reconstruction are convolutional image-generating networks that map an input volume to an output. We choose a fixed input (specifically, we choose it randomly at initialization) and optimize over the weights of the network. The DIP is the first and most popular architecture [Uly+18], and consists of an encoder, decoder and skip connections. The encoder and the skip connections are irrelevant for the performance of the DIP. The Deep Decoder (DD) [HH19] is a simple decoder architecture, even simpler than the decoder part of the DIP. Specifically, the DD only consists of convolutional operations with fixed convolutional filters followed by linear combinations (i.e., 1x1 convolutions). In this paper, we found a variation of the two architectures, that we call ConvDecoder to perform best. The ConvDecoder outperforms the original DIP and DD methods in terms of the reconstruction quality (see Section 5.2). We also tried a variety of other architectures, including combinations of ConvDecoders that reconstruct an image at different resolutions, but again found the simple ConvDecoder to perform best.

4.1 ConvDecoder architecture

ConvDecoder is a convolutional neural network that maps a parameter space to images, i.e., $G: \mathbb{R}^p \rightarrow \mathbb{R}^{c \times w \times h}$, where c is the number of output channels, and w and h are the width and height of the image in each channel. In each layer, except the last one, ConvDecoder is composed of the following components: Nearest-Neighbor up-sampling, a 3x3 convolutional layer, ReLU activation function, and finally a Batch Normalization (BN) block [IS15]. BN normalizes each channel of its input volume independent of other channels. Figure 1 depicts the network.

The parameters of BN and convolutional layers are optimized when fitting the network to the given under-sampled measurement. The final layer excludes the up-sampling layer and simply combines the images via a 1x1 convolutional layer that simply performs linear combinations of the channels.

Convolutional and up-sampling blocks are essential. The former is responsible for capturing local information among the pixels and refines that information from one layer to another. The up-sampling block induces a notion of resolution into each layer. We elaborate upon this notion in Section 4.2. Note that an $(n+1)$ -layer ConvDecoder outputs an image $\hat{\mathbf{x}} \in \mathbb{R}^{c_{n+1} \times w_{n+1} \times h_{n+1}}$ from a fixed input $\mathbf{z} \in \mathbb{R}^{c_0 \times w_0 \times h_0}$ (which is drawn from an arbitrary distribution, e.g. $\sim \mathcal{N}(0, \mathbf{I})$ and then fixed). The default architecture we consider (upon which we slightly tune for each experiment) has 7 layers (including the last layer) and 256 channels per layer.

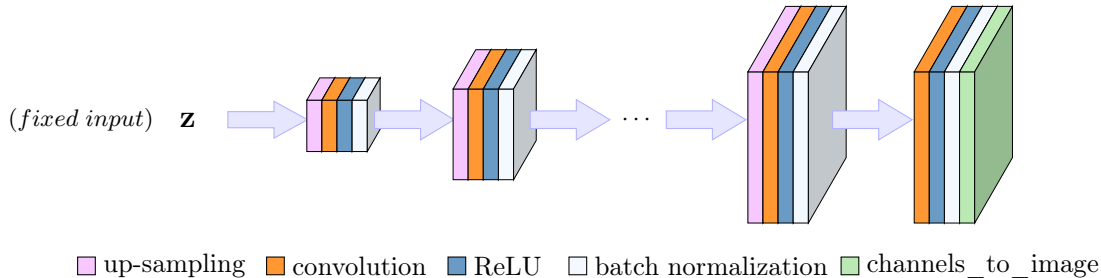


Figure 1: ConvDecoder architecture. It is comprised of up-sampling, convolutional, ReLU, batch normalization, and linear combination layers.

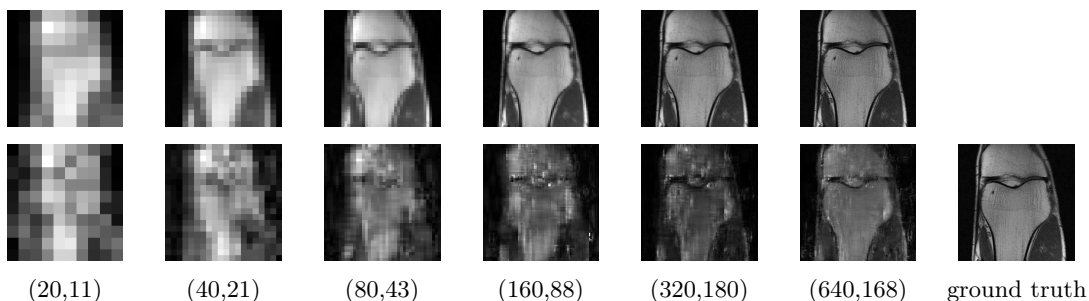


Figure 2: ConvDecoder finds an image representation by constructing fine details per each layer. The network is fitted for representing an image from the 4x under-sampled k -space of the ground-truth image in the mid row. **Top row:** different resolutions of the ground-truth image in the bottom row to each of which we fit the layer outputs. **Bottom row:** output visualization for each of the six layers.

4.2 How does ConvDecoder represent an image?

In order to understand how ConvDecoder functions as an image prior, it is instructive to visualize how it generates an image by visualizing the outputs of each layer. Visualizing the layers' 256 channels, however, is not informative. Instead, we visualize the best representation that can be achieved by linearly combining the channels in each layer to the re-scaled ground-truth image. For example, if the image size (omitting the number of channels) in layer i 's output is (w_i, h_i) , then we down-sample the ground-truth image to match this size.

Figure 2 shows the results of our visualization method. The top row shows different resolutions of the ground-truth image \mathbf{x}_1 . The bottom row shows the visualization results for a network fitted to reconstruct \mathbf{x}_1 from the 4x under-sampled measurements \mathbf{y}_1 . We observe that: (i) ConvDecoder finds a fine representation of an image by adding more detail in each layer. (ii) As shown in Figure 2, we observe the role of up-sampling blocks in inducing the notion of resolution to the network, in that different layers represent reconstructions of different resolutions.

5 Performance of un-trained neural networks for MRI

In this section, we study the performance of un-trained neural networks for multi-coil 4x accelerated MRI reconstruction. We do not study single-coil reconstruction because multi-coil is clinically more relevant. We also study 8x acceleration in Appendix C. Our main findings are: (i) perhaps surprisingly, ConvDecoder performs as well as a standard baseline *trained* method, the U-net, for accelerated MRI—but without any training data, and (ii) ConvDecoder significantly outperforms other un-trained methods in particular total-variation minimization, a standard baseline method.

We performed a grid search to find the best parameters for each method; for the ConvDecoder that resulted in an 8-layer network with 256 channels in each layer. For more details on the architecture setup and optimization parameters, we refer the reader to Appendix B.

5.1 Evaluating reconstruction performance

It is surprisingly non-trivial to compare different reconstruction methods for MRI. We have faced the following challenges and we have made the following choices for measuring reconstruction performance:

Image comparison metrics: Popular image metrics between a ground-truth image and a reconstructed image, like peak-signal-to-noise ratio (PSNR), are often unsuitable to capture reconstruction performance: Mason et al. [Mas+19] have investigated a number of metrics based on the diagnostic quality of MR images according to the feedback given by a group of five radiologists. Their study shows that Visual Information Fidelity (VIF) [SB06] is generally a better metric for assessing diagnostic quality than widely-used metrics such as PSNR and Structural Similarity Index (SSIM) [Wan+04]. Interestingly, PSNR and SSIM—the perhaps most widely-used metrics for assessing image quality—were ranked among the most inept metrics in this study. To conform with common practice, we nevertheless include PSNR and SSIM metrics along with VIF and Multi-Scale SSIM (MS-SSIM) [Wan+03].

Normalization: It is often necessary to normalize images when comparing them to a ground truth image. Marcin et al. [Mar+20] have shown that image normalization techniques have a significant impact on various texture features being extracted from a medical image. We chose mean-std normalization (applied to the ground-truth image to match the statistical properties of the reconstructed image) because the resulting scores were more consistent with the literature.

Comparison to noisy ground truth: In some cases, the ground-truth image itself is corrupted with measurement artifacts. Hence, even if the reconstructed image is of high quality, the score does not reflect that quality and this results in excessive difficulty of comparing different reconstructions. We did not find an automatic way to address this difficulty, other than inspecting images ourselves.

Volume- vs image-based comparison: Finally, all the afore-mentioned metrics are sensitive to whether the comparison is done on an image-based level, or is volume-based (each scan of a knee consists of a number of slices; each slice is an image and together those images form the volume). It is common in the literature [Wan+19; Ram+20; Sri+20b; Sri+20a] that the scores are computed in a volume-based manner, that is, the dynamic range of the volume is considered for computing the scores. However, since images within each volume are analyzed independently, a more reasonable approach is to consider the dynamic range of each image, separately.

To illustrate the point that volume- vs. image-based evaluation gives very different numbers, Table 1 provides average volume-based as well as image-based SSIM and PSNR scores for ConvDecoder, U-net, and TV. Note that the results are averaged over 8 randomly-chosen volumes (256 slice images in total) from the validation set. The numbers show that the image-based score computation results in a lower range of numbers compared with the volume-based one, yet we employ the former because of the afore-mentioned reason. We also refer the reader to Appendix A for further discussion on the mentioned evaluation challenges.

5.2 Evaluation results

We evaluate the performance of ConvDecoder along with other methods on the multi-coil 4x accelerated knee measurements of the FastMRI dataset. As mentioned throughout the paper, we consider three untrained methods, specifically (i) our new ConvDecoder, (ii) DD, and (iii) DIP, (iv) a standard un-trained TV-norm minimization method, and finally (v) the U-net, a standard training based method. We did a grid search to

Method	8 volumes (256 slice images)				200 mid-slice images from 200 volumes			
	Volume-based		Image-based		Image-based			
	SSIM	PSNR	SSIM	PSNR	VIF	MS-SSIM	SSIM	PSNR
ConvDecoder	0.8341	34.43	0.7526	31.11	0.6823	0.9387	0.7753	31.67
U-net	0.8357	34.32	0.7591	31.40	0.5955	0.9489	0.7883	32.04
TV	0.7142	32.90	0.5859	29.85	0.4412	0.9262	0.6977	30.20

Table 1: **Left:** Volume and image based computing leads to different numbers: Average scores for ConvDecoder, U-net, and TV. For comparing volume- vs. image-based evaluation, SSIM and PSNR scores are averaged over 8 randomly-chosen volumes (256 slice images). **Right:** For comparing different methods on the whole dataset (in an image-based manner), 200 mid-slice images from 200 volumes have been considered. All data points are chosen from multi-coil knee measurements of the FastMRI validation set (4x accelerated). ConvDecoder performs best in the VIF metric deemed most relevant by Clinicians. In the other metrics, ConvDecoder and U-net are extremely similar.

select the best parameters for each method, see Appendix B for details and for the parameter setup for each method.

ConvDecoder without training performs as well as a trained U-net and significantly better than an un-trained baseline: We start by comparing ConvDecoder with U-net and TV. To compute the results on the whole validation set, we run the three mentioned methods on the mid-slice image of each volume in the validation set (a set of 200 images over all). Note that U-net is pre-trained on the whole training set (974 volumes). Table 1, right part, shows the results for each method. The scores show that the ConvDecoder has higher VIF performance than U-net, which is deemed most relevant by clinicians, and achieves on-par performance with the U-net according to all metrics. Moreover, it significantly outperforms TV. Figure 3 shows a sample reconstruction for an image from the validation set for the mentioned methods.

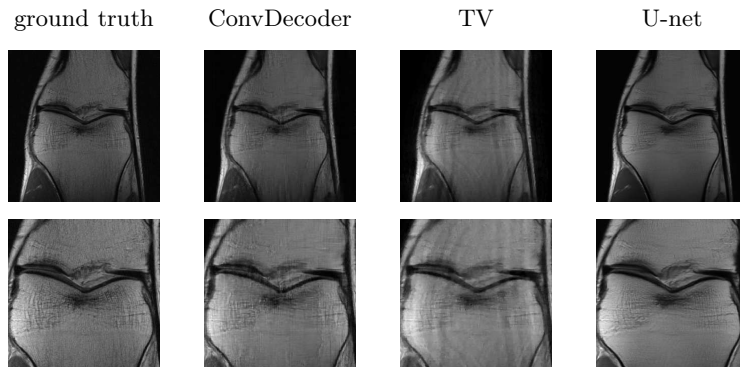


Figure 3: Sample reconstructions for ConvDecoder, TV, and U-net for a validation image from multi-coil knee measurements (4x accelerated). The second row represents zoomed-in version of the first row. ConvDecoder finds the best reconstruction for this image (slightly better than U-net and significantly better than TV).

ConvDecoder outperforms other un-trained neural networks: Next, we compare ConvDecoder with DIP and DD. To compare these methods, we computed the scores by averaging over 20 randomly-chosen mid-slice images of different volumes in the validation set, and as mentioned earlier in this section, they are computed in an image-based manner. Table 2 shows these results and Figure 4 shows two sample reconstructions for each of these methods.

Method	VIF	MS-SSIM	SSIM	PSNR
ConvDecoder	0.6717	0.9443	0.7775	31.81
DIP	0.6311	0.8981	0.5938	28.40
DD	0.6359	0.8599	0.6991	29.16

Table 2: Average image-based scores for the ConvDecoder, DIP, and DD on the mid-slice images of 20 randomly-chosen volumes in the multi-coil knee measurements from the fastMRI validation set (4x accelerated). ConvDecoder significantly outperforms DIP and DD according to all metrics.

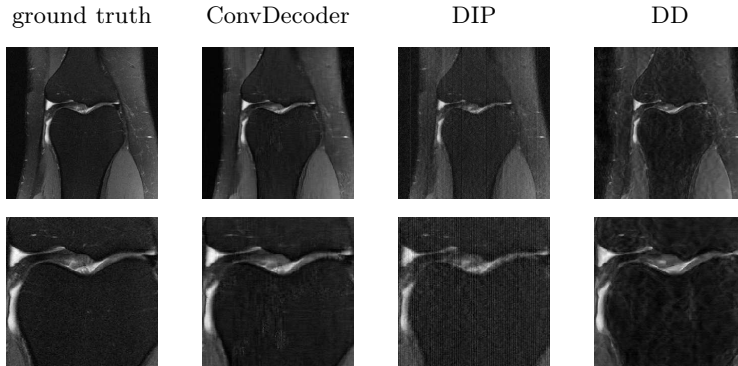


Figure 4: Sample reconstructions for ConvDecoder, DIP, and DD for a validation image from multi-coil knee measurements (4x accelerated). The second row represents zoomed-in version of the first row. ConvDecoder finds the best reconstruction for this image.

From Figure 4, it can be seen that DIP induces a noticeable amount of vertical artifacts and DD—in addition to having reconstruction artifacts—tends to generate rather smooth images and therefore misses texture details. These differences are reflected in other images as well, and hence by averaging the scores over 20 images, in Table 2, we observe a gap between ConvDecoder scores and the scores we obtain from DIP and DD.

5.3 Sensitivity to initialization and choice of hyperparameters

Here, we show (i) how the width of the network affects the reconstruction quality, and (ii) demonstrate that there is little variance in the scores given a specific setup when fitting the ConvDecoder starting from a random initialization to a given under-sampled measurement over multiple runs on the same problem.

A key hyper-parameters of the ConvDecoder is the width of the network (the number of channels per layer). In order to check how different wideness factors affect the performance, we ran a seven-layer ConvDecoder on three under-sampled measurements (again from the multi-coil accelerated knee measurements of the FastMRI dataset) and computed the SSIM score. We performed this experiment four times to average the results. Figure 9 (right) in the Appendix shows the SSIM score based on network width for the three mentioned data points. It can be seen that if the network width is either too small or too large, it does not perform well. A width parameter around 200 performs well across images.

Recall that to recover an image, we run gradient descent starting from a random initialization. It is natural to ask whether the reconstruction quality varies significantly as a function of the random initialization. We find that the reconstruction quality is relatively insensitive to the particular initialization. Specifically, for the general setup we used in Section 5, we ran the ConvDecoder 10 times on an under-sampled measurement and averaged the scores. Figure 9 (left) in the Appendix depicts the variances of different scores over several runs of the algorithm, an illustrate that the scores vary relatively mildly (VIF as well as PSNR and MS-SSIM tend to have the highest and lowest variations, respectively).

6 Robustness to out-of-distribution samples

In Section 5.2, we found that ConvDecoder achieves on-par performance with U-net when evaluating them on the in-distribution samples (i.e., FastMRI validation set). Another aspect to consider for comparing U-net and ConvDecoder is their robustness to out-of-distribution samples.

Un-trained neural networks are robust to a shift in the distribution, as they are *un-trained*, however their optimal hyper-parameters are typically tuned on distribution of images. Trained methods, however, do not enjoy such robustness as they learn a prior from a data distribution. To illustrate this difference, we ran U-net (trained on 4x accelerated knee MRI measurements) and ConvDecoder on an out-of-distribution image (e.g., a non-MRI image). We used the same 4x accelerated mask (as in the MRI reconstruction problem) for under-sampling the frequency-domain representation of this image. Figure 5 shows that the ConvDecoder significantly outperforms U-net when it comes to evaluation on the out-of-distribution samples.

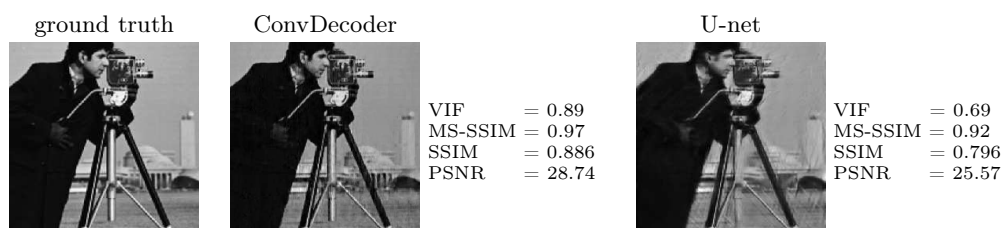


Figure 5: Un-trained methods are robust to a shift in the distribution. Both methods are run for 4x under-sampled (in the frequency domain) version of the cameraman test image. U-net is trained on 4x accelerated multi-coil knee measurements from the FastMRI dataset.

7 Broader impact

Deep learning methods are being used increasingly frequently for medical imaging in practice, for example GE’s TrueFidelity, deep learning based reconstruction algorithm for CT imaging, has FDA approval since 2019. Deep networks are typically used for their superior reconstruction performance over classical methods, but two major concerns when applying them in clinical practice are i) they might fantasize parts of an image based on the training data and ii) that they are sensitive to a shift in distribution, thus when trained on one patient population or scanner technology, they might perform worse when tested on another patient population or scanner technology. Un-trained networks, in contrast, don’t have those two shortcomings, but they are not thought to be able to compete with trained deep networks in reconstruction performance. Our work shows that they can compete with trained methods, at least with a strong baseline (the U-net). The best trained neural networks probably still outperform our un-trained one, but we hope that our finding will motivate further research and improvements of un-trained methods, and establish them as a stable method besides trained neural networks for image reconstruction.

Code

Code to reproduce the experiments is available at <https://github.com/MLI-lab/ConvDecoder>.

Acknowledgements

R. Heckel and M. Zalbagi Darestani are partially supported by NSF award IIS-1816986, and R. Heckel acknowledges support of the NVIDIA Corporation in form of a GPU, and is partially supported by the IAS at TUM.

References

- [Agu+17] E. Agustsson, F. Mentzer, M. Tschannen, L. Cavigelli, R. Timofte, L. Benini, and L. V. Gool. “Soft-to-hard vector quantization for end-to-end learning compressible representations”. In: *Advances in Neural Information Processing Systems (NeurIPS)*. 2017, pp. 1141–1151.
- [Aro+20] S. Arora, V. Roeloffs, and M. Lustig. “Untrained modified deep decoder for joint denoising parallel imaging reconstruction”. In: *International Society for Magnetic Resonance in Medicine Annual Meeting*. 2020.
- [Blo+07] K. T. Block, M. Uecker, and J. Frahm. “Undersampled radial MRI with multiple coils. Iterative image reconstruction using a total variation constraint”. In: *Magnetic Resonance in Medicine: An Official Journal of the International Society for Magnetic Resonance in Medicine*. 2007, pp. 1086–1098.
- [Bor+17] A. Bora, A. Jalal, E. Price, and A. G. Dimakis. “Compressed sensing using generative models”. In: *International Conference on Machine Learning (ICML)*. 2017, pp. 537–546.
- [Bos+20] E. Bostan, R. Heckel, M. Chen, M. Kellman, and L. Waller. “Deep phase decoder: self-calibrating phase microscopy with an untrained deep neural network”. In: *Optica*. 2020, pp. 559–562.
- [Bur+12] H. C. Burger, C. J. Schuler, and S. Harmeling. “Image denoising: can plain neural networks compete with BM3D?” In: *IEEE Conference on Computer Vision and Pattern Recognition*. 2012, pp. 2392–2399.
- [HH19] R. Heckel and P. Hand. “Deep Decoder: concise image representations from untrained non-convolutional networks”. In: *International Conference on Learning Representations (ICLR)*. 2019.
- [HS20a] R. Heckel and M. Soltanolkotabi. “Denoising and regularization via exploiting the structural bias of convolutional generators”. In: *International Conference on Learning Representations (ICLR)*. 2020.
- [HS20b] R. Heckel and M. Soltanolkotabi. “Compressive sensing with un-trained neural networks: Gradient descent finds the smoothest approximation”. In: *International Conference on Machine Learning (ICML)*. 2020.
- [HA20] R. Hyder and M. S. Asif. “Generative models for low-dimensional video representation and reconstruction”. In: *IEEE Transactions on Signal Processing*. 2020, pp. 1688–1701.
- [IS15] S. Ioffe and C. Szegedy. “Batch Normalization: accelerating deep network training by reducing internal covariate shift”. In: *International Conference on Machine Learning (ICML)*. 2015, pp. 448–456.
- [JH19] G. Jagatap and C. Hegde. “Algorithmic guarantees for inverse imaging with untrained network priors”. In: *Advances in Neural Information Processing Systems (NeurIPS)*. 2019.
- [Jin+19] K. H. Jin, H. Gupta, J. Yerly, M. Stuber, and M. Unser. “Time-dependent deep image prior for dynamic MRF”. In: *arXiv:1910.01684 [eess.IV]*. 2019.
- [KB15] D. P. Kingma and J. Ba. “Adam: a method for stochastic optimization”. In: *International Conference on Learning Representations (ICLR)*. 2015.
- [Mar+20] K. Marcin, S. Michał, and O. Rafał. “Does image normalization and intensity resolution impact texture classification?” In: *Computerized Medical Imaging and Graphics*. 2020, p. 101716.
- [Mas+19] A. Mason, J. Rioux, S. E. Clarke, A. Costa, M. Schmidt, V. Keough, T. Huynh, and S. Beyea. “Comparison of objective image quality metrics to expert radiologists’ scoring of diagnostic quality of MR images”. In: *IEEE Transactions on Medical Imaging*. 2019, pp. 1064–1072.
- [PW19] P. Putzky and M. Welling. “Invert to learn to invert”. In: *Advances in Neural Information Processing Systems (NeurIPS)*. 2019, pp. 444–454.

- [Ram+20] Z. Ramzi, P. Ciuciu, and J. L. Starck. “Benchmarking deep nets MRI reconstruction models on the FastMRI publicly available dataset”. In: *International Symposium on Biomedical Imaging*. 2020.
- [Ron+15] O. Ronneberger, P. Fischer, and T. Brox. “U-net: convolutional networks for biomedical image segmentation”. In: *International Conference on Medical Image Computing and Computer-Assisted Intervention*. 2015, pp. 234–241.
- [Sch+17] J. Schlemper, J. Caballero, J. V. Hajnal, A. Price, and D. Rueckert. “A deep cascade of convolutional neural networks for MR image reconstruction”. In: *International Conference on Information Processing in Medical Imaging*. 2017, pp. 647–658.
- [SB06] H. R. Sheikh and A. C. Bovik. “Image information and visual quality”. In: *IEEE Transactions on Image Processing*. 2006, pp. 430–444.
- [Sri+20a] A. Sriram, J. Zbontar, T. Murrell, A. Defazio, C. L. Zitnick, N. Yakubova, F. Knoll, and P. Johnson. “End-to-end variational networks for accelerated MRI reconstruction”. In: *arXiv:2004.06688 [eess.IV]*. 2020.
- [Sri+20b] S. Sriram, J. Zbontar, T. Murrell, C. L. Zitnick, A. Defazio, and D. K. Sodickson. “GrappaNet: combining parallel imaging with deep learning for multi-coil MRI reconstruction”. In: *IEEE/CVF Conference on Computer Vision and Pattern Recognition*. 2020, pp. 14315–14322.
- [The+17] L. Theis, W. Shi, A. Cunningham, and F. Huszár. “Lossy image compression with compressive autoencoders”. In: *International Conference on Learning Representations (ICLR)*. 2017.
- [Tod+15] G. Toderici, S. M. O’Malley, S. J. Hwang, D. Vincent, D. Minnen, S. Baluja, M. Covell, and R. Sukthankar. “Variable rate image compression with recurrent neural networks”. In: *International Conference on Learning Representations (ICLR)*. 2015.
- [Uly+18] D. Ulyanov, A. Vedaldi, and V. Lempitsky. “Deep image prior”. In: *IEEE Conference on Computer Vision and Pattern Recognition*. 2018, pp. 9446–9454.
- [Vee+18] D. V. Veen, A. Jalal, M. Soltanolkotabi, E. Price, S. Vishwanath, and A. G. Dimakis. “Compressed sensing with deep image prior and learned regularization”. In: *arXiv:1806.06438 [stat.ML]*. 2018.
- [Wan+20] F. Wang, Y. Bian, H. Wang, M. Lyu, G. Pedrini, W. Osten, G. Barbastathis, and G. Situ. “Phase imaging with an untrained neural network”. In: *Light: Science & Applications*. 2020, pp. 1–7.
- [Wan+19] P. Wang, E. Z. Chen, T. Chen, V. M. Patel, and S. Sun. “Pyramid convolutional RNN for MRI reconstruction”. In: *arXiv: 1912.00543 [eess.IV]*. 2019.
- [Wan+04] Z. Wang, A. C. Bovik, H. R. Sheikh, and E. P. Simoncelli. “Image quality assessment: from error visibility to structural similarity”. In: *IEEE Transactions on Image Processing*. 2004, pp. 600–612.
- [Wan+03] Z. Wang, E. P. Simoncelli, and A. C. Bovik. “Multiscale structural similarity for image quality assessment”. In: *Asilomar Conference on Signals, Systems & Computers*. 2003, pp. 1398–1402.
- [Ye19] J. C. Ye. “Compressed sensing MRI: a review from signal processing perspective”. In: *BMC Biomedical Engineering*. 2019, pp. 1–17.
- [Zbo+18] J. Zbontar, F. Knoll, A. Sriram, M. J. Muckley, M. Bruno, A. Defazio, M. Parente, K. J. Geras, J. Katsnelson, H. Chandarana, et al. “FastMRI: An open dataset and benchmarks for accelerated MRI”. In: *arXiv: 1811.08839 [cs.CV]*. 2018.

APPENDIX

A More details on evaluating reconstruction performance

As mentioned in Section 5.1, evaluating the performance of different reconstruction methods is challenging for reasons related to the (i) choice of image comparison metrics, (ii) impact of the normalization of images, (iii) the fact that we often compare to a noisy ground truth image, and (iv) because we can compare image wise or volume wise. In this section, we further iterate points ii and iii.

Normalization: As for the image normalization type, which is typically required to fairly compare two images, we investigated three image normalization methods: min-max normalization, which transforms image I to $\frac{I - \min(I)}{\max(I) - \min(I)}$; mean-std normalization on both ground-truth and reconstructed images, which transforms image I to $\frac{I - \text{mean}(I)}{\text{std}(I)}$; and mean-std normalization which is only applied to the ground-truth image to match its histogram to that of the reconstructed image.

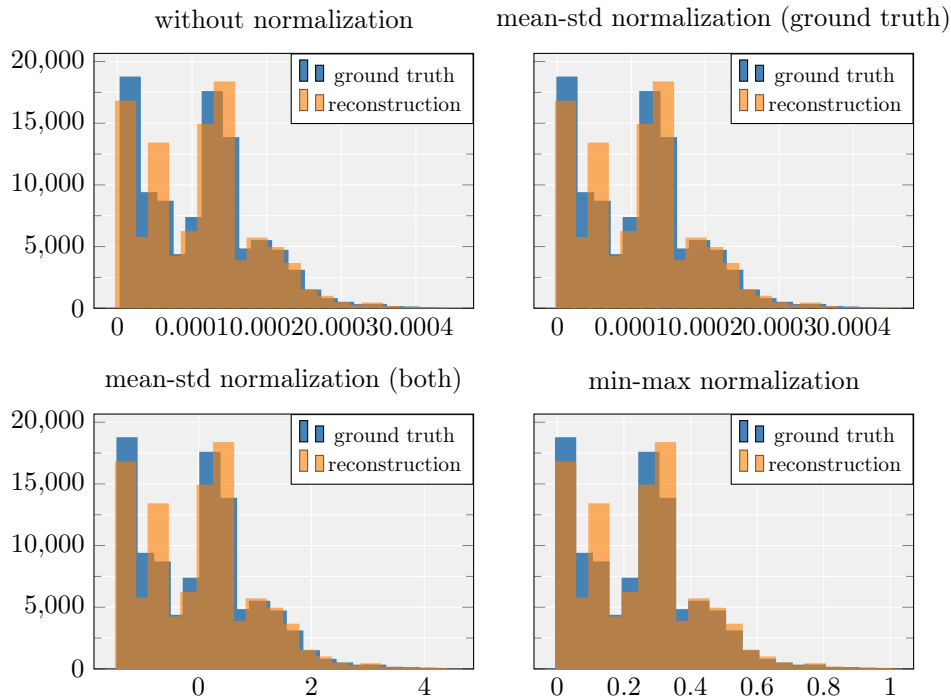


Figure 6: The effect of different image normalization techniques on the distribution of ground truth and reconstructed images.

Figure 6 illustrates how each of the mentioned normalization methods affect the distribution of ground-truth and reconstructed images for a sample file from the multi-coil knee dataset. In addition, Table 3 shows the average SSIM and PSNR scores for ConvDecoder, Unet, and TV after running them on 200 mid-slice images from the multi-coil knee dataset (4x accelerated). The remarkable outcome of these results is that different image normalization methods can result in a totally different winning reconstruction method.

Comparison to noisy ground truth: As mentioned, in some cases the ground-truth image itself is corrupted with measurements images, as illustrated in Figure 7 where the ground truth image is very noisy. In

Method	no norm		min-max		mean-std (both)		mean-std (gt)	
	SSIM	PSNR	SSIM	PSNR	SSIM	PSNR	SSIM	PSNR
ConvDecoder	0.7563	29.93	0.7464	30.09	0.6957	29.57	0.7753	31.67
U-net	0.7867	32.01	0.7354	28.04	0.7091	29.37	0.7883	32.04
TV	0.6592	27.21	0.6875	26.67	0.6565	28.43	0.6977	30.20

Table 3: Average image-based scores for the ConvDecoder, U-net, and TV on the mid-slice images of the volumes in the multi-coil knee measurements from the fastMRI validation set (4x accelerated). Scores are computed based on different image normalization methods. Surprisingly, different image normalization types may result in a totally different winning reconstruction method.

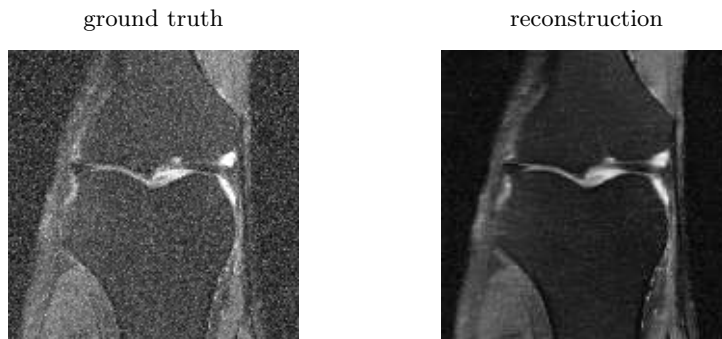


Figure 7: A sample image from the multi-coil knee dataset where the ground-truth image is very noisy. In the evaluation, we compare a reconstructed image to such a noisy image, and even if the reconstruction is a subjectively sharp and clear image, the error metric is large.

such cases, the scores do not reflect the true quality of the reconstructed image. Note that the reconstruction is almost free from noise, demonstrating the image prior also denoises the image.

B Parameter setup

We manually tuned the parameters of ConvDecoder, DIP, and DD by performing a grid search and observing their performance on a group of 10 randomly-chosen images.

Table 4 shows the grid parameters for each network. For the U-net (and also TV), we chose the set of parameters used in the FastMRI challenge¹ [Zbo+18]. The parameter setup is provided in Table 5.

Method	layers	channels	residuals
ConvDecoder	{6, 7, 8, 9}	{160, 256, 480}	-
DIP	{12, 14, 16, 18}	{160, 256, 360}	{2, 4}
DD	{6, 7, 8, 9, 10}	{256, 368, 512}	-

Table 4: Grid-search parameters for ConvDecoder, DIP, and DD.

In order to fit the un-trained methods to the under-sampled measurements, we used the adam optimizer [KB15] with constant learning rate 0.01 (without early stopping) for optimizing the loss function (which is MSE loss function in our experiments).

¹<https://github.com/facebookresearch/fastMRI/tree/master/models>

Method	#layers	#channels (or width)	convolutional kernel size	#residuals
ConvDecoder	8	256	3	0
U-net	8	32*	3	4
DIP	16	256	3	2
DD	10	368	1	0

* This is the number of channels for the first layer of U-net. For the 8-layer U-net that we used, the number of channels are [32, 64, 128, 256, 512, 256, 128, 64, 32] including a non-pooling layer in the middle.

Table 5: Model parameters for ConvDecoder, U-net, DIP, and DD.

Regarding the output dimension of un-trained methods, as an example, for a $15 \times 640 \times 368$ (15 is the number of coils) under-sampled measurement, ConvDecoder (also DIP or DD) generates an image of size $30 \times 640 \times 368$, because it recovers the real and complex pixel values of an image separately with two separate channels. Finally, we fixated the input of the un-trained methods which is sampled from $\mathcal{N}(0, I)$ and has dimension $256 \times 10 \times 5$ (256 being the number of channels).

C 8x acceleration

We have seen in Section 5.2 that ConvDecoder achieves on-par performance with U-net and significantly outperforms TV-norm minimization for the 4x accelerated multi-coil reconstruction task. Here, we consider 8x acceleration as a higher acceleration factor.

Method	layers	channels	input size
ConvDecoder	{6*, 7, 9}	{64*, 128, 256, 380}	{(4,4)*, (8,8), (16,16), (32,32)}

* Selected by grid search.

Table 6: Grid-search parameters for ConvDecoder (8x acceleration).

For 8x acceleration, we found different hyper-parameters of the ConvDecoder (relative to 4x acceleration) to work best. To find good hyper-parameters for the ConvDecoder, we randomly picked 6 images and performed a grid search over the grid parameters shown in table 6. We sorted all sets of parameters based on all four metrics. Afterward, we picked 3 sets of parameters that appeared in the top-5 best-performing hyper-parameter configurations according to all metrics. Finally, we selected one out of the three best-performing hyper-parameter configurations by running the three hyper-parameter configurations on 6 more (randomly-chosen) images (the selected setup outperformed the other two based on all metrics).

Method	VIF	MS-SSIM	SSIM	PSNR
ConvDecoder	0.5234	0.8827	0.6815	28.49
U-net	0.5233	0.9148	0.7115	29.25
TV	0.3119	0.8340	0.5986	26.55

Table 7: Average image-based scores for the ConvDecoder, U-net, and TV on the mid-slice images of 200 volumes in the multi-coil knee measurements from the FastMRI validation set (8x accelerated). ConvDecoder achieves on-par performance with U-net and outperforms TV.

Table 7 shows the scores for ConvDecoder, U-net, and TV. ConvDecoder achieves similar performance with U-net (according to all metrics except SSIM and MS-SSIM which U-net slightly outperforms ConvDe-

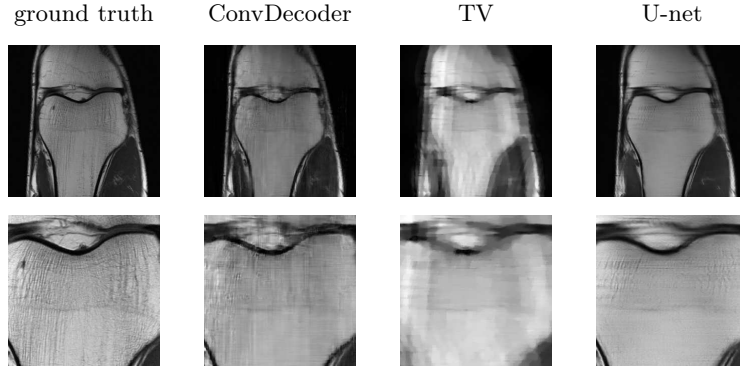


Figure 8: Sample reconstructions for ConvDecoder, TV, and U-net for a validation image from multi-coil knee measurements (8x accelerated). The second row represents zoomed-in version of the first row. ConvDecoder finds a similar reconstruction as U-net and outperforms TV.

coder) and significantly outperforms TV. Figure 8 shows a sample reconstruction for the three mentioned methods. Those experiments for 8x acceleration second our finding for 4x acceleration that the structure of the network is a sufficient prior for the MRI compressed sensing task, at least when considering a baseline trained method (U-net) for comparison.

D Sensitivity to initialization and choice of hyperparameters

Figure 9 was discussed in Section 5.3. Figure 9, left panel, depicts the image metrics as a function of the random initialization, and shows they they vary relatively mildly over runs of the algorithms. Figure 9, right panel, shows the SSIM score as a function of network width, and demonstrates that the error is large both if the network is not wide enough and if it is too wide.

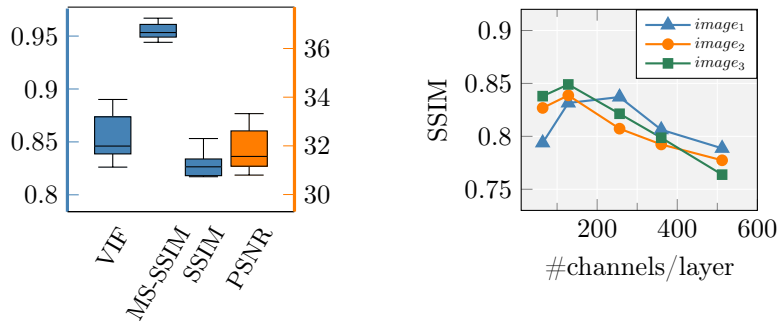


Figure 9: Effect of hyper-parameters on the ConvDecoder's performance. **Left:** fluctuations of different scores during 10 runs on a single data point. **Right:** effect of network width on the SSIM score for three data points from the validation set.